Magnetism and chemical ordering in icosahedral Al-Pd-Mn quasicrystal

M. Krajčí[1,2] and J. Hafner[2]
[1]*Institute of Physics, Slovak Academy of Sciences, Dúbravská cesta 9, SK-84511 Bratislava, Slovak Republic*
[2]*Fakultät für Physik and Center for Computational Materials Science, Universität Wien, Sensengasse 8/12, A-1090 Wien, Austria*
(Received 2 October 2008; revised manuscript received 27 November 2008; published 30 December 2008)

Even after nearly two decades of research efforts, the origin of the outstanding magnetic properties of icosahedral quasicrystals containing Mn remains unclear. Experiments have demonstrated that only a rather small fraction of the Mn atoms carry rather large magnetic moments, but it remains unclear whether these sites are intrinsic to the quasicrystalline structure or represent defects. We present *ab initio* density-functional calculations of the magnetic properties of a large 2/1 approximant to icosahedral (*i*) Al-Pd-Mn, performed in the semilocal generalized gradient approximation. Structures for rational approximants to the quasicrystalline structure of bulk *i*-Al-Pd-Mn have been constructed using the cut-and-projection technique in six-dimensional (6D) hyperspace according to the Katz-Gratias-Boudard model. We studied magnetism in models of the 2/1 approximant with idealized coordinates obtained by projection from 6D hyperspace in models with coordinates relaxed using Hellmann-Feynman forces and in models simulating the structure of the quasicrystal at high temperature. In some idealized structural models a majority of the Mn atoms carry a large magnetic moment. Although this contradicts experiments demonstrating that only a very small fraction of the Mn atoms are magnetic, this provides the opportunity to investigate in detail the mechanisms leading to the formation of magnetic moments on the Mn atoms. We identify two major mechanisms: a loosely packed environment of the Mn atoms and a direct Mn-Pd interactions leading to a shift of the Mn *d* band toward the Fermi level. The dominant contribution is the Mn-Pd interaction. A large magnetic moment on a Mn atom is formed at special sites where the Mn atom has two or three Pd nearest neighbors. These special sites are located at those regions of the quasiperiodic lattice where the pseudo-Mackay and Bergman clusters building the structure are linked along the threefold axes. At these sites, the building principles of the Mackay and Bergman clusters are in conflict: from the side of the Mackay cluster, occupation with an Al atom is required, whereas the symmetry of the Bergman cluster suggests occupation by a Pd atom. We have found that a small modification of the chemical decoration of these sites (corresponding to a slight modification of the internal shell structure of the occupation domains in the 6D hyperspace) can lead to a complete disappearance of magnetism in *i*-Al-Pd-Mn. Total energy calculations show that models with a chemical ordering disfavoring formation of magnetic moments on Mn atoms have the lowest energies. This re-establishes agreement with experiment. The ground state of *i*-Al-Pd-Mn is nonmagnetic; but at these specific sites, Al atoms can be replaced by Pd at low energetic cost and without strong violation of the building principles of the quasicrystalline structure, resulting in the formation of large local magnetic moments.

DOI: 10.1103/PhysRevB.78.224207 PACS number(s): 61.44.Br, 71.23.Ft, 75.50.Kj

I. INTRODUCTION

The magnetic properties of quasicrystals continue to be a fascinating field of research. In general, in quasicrystals magnetic moments are found only on a small minority of atoms. In quasicrystals formed by Al with Ni and Co, the 3*d* atoms are nonmagnetic, suggesting that the geometric and electronic structures of quasicrystals disfavor magnetic-moment formation.[1] But in quasicrystals containing Mn, localized magnetic moments on the Mn atoms have been detected systematically since the pioneering work of Hauser *et al.*,[1] published very shortly after the discovery of quasicrystalline phases in the Al-Mn system.[2] Above a temperature of about 5 K, the magnetic susceptibility χ measured in a weak magnetic field was found to follow a Curie-Weiss law, $\chi \propto C/(T+\Theta)$, in AlMn and AlSiMn quasicrystals with a Mn content varying between 14 and 22 at. %. This suggests the existence of local moments. At very low temperatures, the temperature-dependent susceptibility measured in a weak alternating (ac) field displays a peak at $T_f \leq 5$ K. This proves the existence of magnetic interactions between the local moments, and it was proposed that quasicrystals show spin-glass behavior. An intriguing observation was the smallness of the Curie constant *C*. The Curie constant is proportional to $xN_{\mathrm{Mn}}S(S+1)$, where N_{Mn} is the total number of Mn atoms, *x* stands for the fraction of Mn atoms carrying a magnetic moment, and *S* is their spin. If it is assumed that all Mn atoms carry the maximal spin of $S=5/2$ compatible with Hund's rules, it follows that only a very low percentage of the Mn atoms in the quasicrystal are magnetic. This observation was soon confirmed by nuclear magnetic resonance (NMR) experiments of Warren *et al.*[3] who concluded that most Mn atoms are nonmagnetic—in agreement with the low value of the Curie constant deduced from the susceptibility measurements. The same observations (small Curie constant, peak in the ac susceptibility, and low concentration of magnetic Mn atoms) were also reported for other quasicrystalline phases containing Mn: metastable decagonal AlMn,[4] stable icosahedral Al-Pd-Mn,[5,6] and decagonal Al-Pd-Mn.[7,8]

Hence the following questions arise: Why are most Mn atoms nonmagnetic? What is the magnetic moment of the magnetic Mn atoms? Do the magnetic atoms belong to the

quasicrystalline phase or are they located in another magnetic phase? If the magnetic atoms belong to the quasicrystalline phase, are they located at specific sites, intrinsic to the quasiperiodic structure, or are magnetic moments formed only at defects in the quasiperiodic lattice? An extensive study[5,9] of magnetism performed on 14 different samples of icosahedral Al-Pd-Mn, cut from single-grain specimens (and hence excluding the presence of a second phase or grain boundaries where Mn moments could be formed), sheds some light on this last question. The magnetization was found to be dependent on thermal treatment and composition. (i) The slower the cooling rate (and hence the better the structural homogeneity), the lower the concentration of magnetic atoms. (ii) A minimum of the magnetization was located at a composition of about 7.75 at. % Mn and 21.9 at. % Pd. The concentration of magnetic atoms increases strongly when the Mn or the Pd content changes. These results have been interpreted as indicating that magnetic Mn atoms are not located at specific sites but associated with defective local arrangements of the transition-metal species. It has been conjectured that at an ideal composition the quasicrystal could be entirely nonmagnetic provided the structure has been fully relaxed.

A number of attempts have been made to use spin-polarized density-functional theory to predict the magnetic properties of icosahedral Al-Pd-Mn and of related crystalline, liquid, and amorphous phases. For orthorhombic Al_6Mn we[10] have shown that the ground state is nonmagnetic. A similar conclusion has been reached by Hippert *et al.*[11] for $Al_{12}Mn$, β-Al_9Mn_3Si, and α-AlMnSi (which is a cubic 1/1 approximant to the quasicrystal). In contrast, the existence of localized moments on a small fraction of the Mn atoms has been reported, based on both experiment and theory, for the hexagonal Al_4Mn phase.[12] On the basis of an analysis of the spin-dependent Mn-Mn pair interactions derived from perturbation theory it was suggested[13] (although without confirmation by *ab initio* electronic structure calculations) that only the Mn site with the lowest coordination [seven Al atoms on an only partially occupied coordination polyhedron and no Mn nearest-neighbor-Wyckoff site (2*a*) in Ref. 14] carries a magnetic moment. An isolated Mn atom on a substitutional site in face-centered-cubic aluminum carries a large magnetic moment,[15] and dilute substitutional alloys of Mn in Al show a spin-glass-like distribution of magnetic moments.[10] The investigation of moment formation in quasicrystalline approximants is hampered by the low concentration of magnetic sites. For 1/1 and 2/1 approximants to icosahedral Al-Pd-Mn, with 128 and 544 atoms/cells, respectively, calculations in the local spin-density approximation (LSDA) found only small magnetic moments of the order of $0.1\mu_B$.[10] The investigations have also been extended to the 3/2 approximant with 2292 atoms/cell (out of them 208 atoms are Mn, distributed over 20 inequivalent sites). A large magnetic moment of $2.4\mu_B$ was found only on a single type of Mn sites characterized by a low Mn-Al coordination and three Mn-Pd neighbors (note that there are no direct Mn-Mn neighbors in any of the icosahedral approximants).[16] Calculations on low-order approximants to decagonal Al-Pd-Mn (*T*- and *R*-phases and their τ^2-rescaled variants) proposed by Hiraga *et al.*[17,18] show a slightly different picture. The decagonal approximants are characterized by some close Mn-Mn neighbors and a looser Mn-Al packing, both favoring moment formation on a very few selected sites. However, spin-polarized calculations converge only to modest magnetic moments ($0.3\mu_B$ to $1\mu_B$) on a few sites. In contrast, large magnetic moments fluctuating between $-1.8\mu_B$ and $+2.7\mu_B$ where found on about 16% of the Mn atoms in liquid $Al_{0.86}Mn_{0.14}$ alloys, while the remaining Mn atoms show only modest moments $|m| \leq 0.2\mu_B$.[10] That most Mn atoms in liquid AlMn or Al-Pd-Mn carry a magnetic moment was also confirmed by experiment[19] and recent *ab initio* molecular-dynamics simulations.[20] The combined analysis of the results on all these different phases has led to two main conclusions. (i) Moment formation is determined by the Stoner criterion for itinerant magnetism—a magnetic moment is formed on those sites where the local paramagnetic density of states (DOS) exceeds the critical value of ≈ 2 states/eV. The local magnetic moments m_i and exchange splitting Δ_i in all materials follow an exactly linear correlation, $\Delta_i = I m_i$, with a universal value of the Stoner parameter, $I \sim 0.9$ eV/μ_B (which agrees with the value determined, both theoretically and experimentally, for many crystalline and amorphous magnetic alloys[21,22]). (ii) A high local paramagnetic DOS and hence formation of a magnetic moment is favored by two mechanisms: a loose coordination of the Mn atoms and the presence of transition-metal atoms in the nearest-neighbor shell.

In our previous work[16] it was shown that no sites with large Mn moments are found in the 1/1 and 2/1 approximants; in the 3/2 approximant a large magnetic moment is found only on a single set of crystallographic sites (out of 20), corresponding to 12 magnetic Mn atoms out of 208. However, it remains unclear whether moment formation on this site is an intrinsic property of the icosahedral structure or an artifact related to special local coordinations in this approximant. In addition we have to emphasize that (i) the calculations have been performed on a model with idealized coordinates, using tight-binding linear muffin-tin orbital (LMTO) techniques. The idealized coordinates mean that, since they are calculated without regard to the size of the atomic species decorating the lattice, an unrealistically loose packing might exist around of some of the Mn atoms (Mn is smaller than either Pd or Al). (ii) The calculations have been performed in the LSDA. Since then we have learned that the LSDA fails to produce a correct description of the ground state of important magnetic materials; Fe is found to be nonmagnetic and hexagonal-close packed instead of ferromagnetic and body-centered cubic,[23] and Cr and Mn are predicted to be nonmagnetic instead of antiferromagnetic.[24] The correct magnetic ground state is found only when the calculations use the semilocal generalized gradient approximation (GGA) to the exchange-correlation functional.

In the present work, we use density-functional calculations not only to determine the electronic structure but also to perform an optimization of the geometric structure using the Hellmann-Feynman forces acting on the atoms. The exchange-correlation functional is treated in the GGA. We perform a detailed investigation of the chemical decoration of the lattice structure of the approximants as determined by the shell structure of the acceptance domain in six-dimensional (6D) space. Different chemical variants, differ-

ing only by modest changes in the shell structure of the atomic surfaces, and their magnetic properties are investigated. The central result of our study is that moment formation on the Mn atoms depends critically on the existence of two or more Pd atoms on nearest-neighbors sites. Interestingly, these are precisely the sites in the lattice where chemical decoration predicted by the shell structure of the acceptance domains and by the building principle of the icosahedral lattice in terms of interpenetrating Bergman and Mackay clusters are in conflict. The concentration of magnetic sites varies with the occupation of these sites with Pd or Al atoms; we find that the acceptable configurations (as determined by their total energies) lead to magnetizations covering precisely the range determined by experiments on many different samples, with a nonmagnetic configuration having the lowest energy.

II. SPIN-POLARIZED DENSITY-FUNCTIONAL CALCULATIONS

All calculations were performed using the Vienna *ab initio* simulation package (VASP) (Refs. 25–27) performing an iterative solution of the Kohn-Sham equations of density-functional theory (DFT) within a plane-wave basis. Both a local and a gradient-corrected functional[28,29] (PW91) were used to describe electronic exchange and correlation. The projector augmented wave (PAW) method[30,31] was used to describe the electron-ion interactions. For valence electrons a plane-wave basis set was employed with an energy cutoff of 400 eV. Since the unit cell of the 2/1 approximant is very large (containing 544 atoms), the calculations were performed for the Γ point only. The paramagnetic densities of states were calculated on a $2\times2\times2$ mesh in the Brillouin zone. In spin-polarized calculations the spin interpolation of Vosko *et al.*[32] was used. A static relaxation of the idealized structure of the approximant was performed using a quasi-Newton technique. Local magnetic moments have been calculated by projecting the plane-wave components of the spin-polarized eigenstates on spherical waves within atomic spheres and integrating the resulting local spin-polarized densities of states up to the Fermi level. The atomic-sphere radius has been chosen such that the local moments sum up to the correct value for the total moment.

A. Magnetic moments on Mn atoms: From the isolated atom to alloys

According to Hund's rules a free Mn atom has a spin of $S=5/2$ and zero orbital moment. The crystalline and magnetic ground state of solid metallic Mn is very complex, with a crystal structure with 58 atoms per unit cell and a noncollinear antiferromagnetic spin structure. These strange properties arise from the conflicting tendencies to simultaneously maximize magnetic moment (according to Hund's rule) and bond strength (as expected from a half-filled d band where only bonding and no antibonding states are occupied). The geometric and magnetic structure of α-Mn represents a compromise; it may be considered as an intermetallic compound between strongly and weakly magnetic Mn atoms, noncollinearity resulting from a topological frustration of the antiferromagnetic nearest-neighbor exchange interactions.[33] In the slightly less stable β phase, topological frustration even leads to spin-liquid behavior down to the lowest temperatures.[34,35] Face-centered-cubic δ-Mn is instable against tetragonal distortion, forming two nearly degenerate antiferromagnetic phases with $c/a<1$ and $c/a>1$; body-centered-cubic γ-Mn forms spin spirals with energies slightly below the collinear antiferromagnetic state, while hexagonal-close-packed ϵ-Mn is nonmagnetic.[34,36] We mention these results to emphasize how strongly the magnetic properties on Mn can vary, depending on the geometry of the environment. DFT calculations in the GGA yield a very satisfactory description of the various crystalline and magnetic phases on Mn,[33–36] while LSDA calculations find a nonmagnetic and hexagonal ground state.[37]

The complexity of the magnetic exchange interactions between Mn atoms is also reflected in the properties of alloys of Mn with other magnetic or nonmagnetic metals. The ground state of face-centered tetragonal Ni-Mn compounds is antiferromagnetic with large moments ($\pm3.4\mu_B$) on the Mn atoms, while the magnetic moments on the Ni atoms are completely quenched due to frustration.[38] Ordered γ-FeMn alloys have a noncollinear magnetic ground state determined by competing ferromagnetic and antiferromagnetic interactions, while substitutional disorder favors the formation of a collinear layered antiferromagnetic structure.[39] In dilute alloys with Al and Mn, *ab initio* calculations converge to a spin-glass-like distribution of the magnetic moments.[10,40]

A difficult aspect of spin-polarized calculations of dilute Mn alloys is the initialization of the local magnetic moments. The work on Mn-Cu and Mn-Al spin glasses has shown that different initializations can lead to the formation of different metastable magnetic configurations; to determine the ground state, a rather extended search in configuration space is required. For the quasicrystalline alloys this means that one has to guess on which site a large magnetic moments is likely to be formed. An alternative to the initialization of magnetic moments is to perform a fixed moment calculation The total magnetic moment M per cell is constrained to a fixed value by adding the constraint by a Lagrange multiplier λ, the total energy being given by[41]

$$E(M)=\min\left[E\{n(\vec{r}),m(\vec{r})\}+\lambda\left(\int_V m(\vec{r})d^3r-M\right)\right].$$

Here $n(\vec{r})$ and $m(\vec{r})$ represent the charge and spin densities of the system and physically the Lagrange multiplier λ represents a magnetic field acting on the electrons. Alternatively, the difference in the number of electrons occupying the spin-up and spin-down eigenstates (and hence the magnetic moment M) may be constrained to a fixed value.[42,43] Here we follow the computationally less demanding approach of Williams *et al.*[42] to fix the occupation number in the two spin channels.

Figure 1 shows the total magnetic energy of the 2/1 approximant to icosahedral Al-Pd-Mn (details of the structure are given below) as a function of the magnetic moment, as calculated in the LSDA and in the GGA. The results demon-

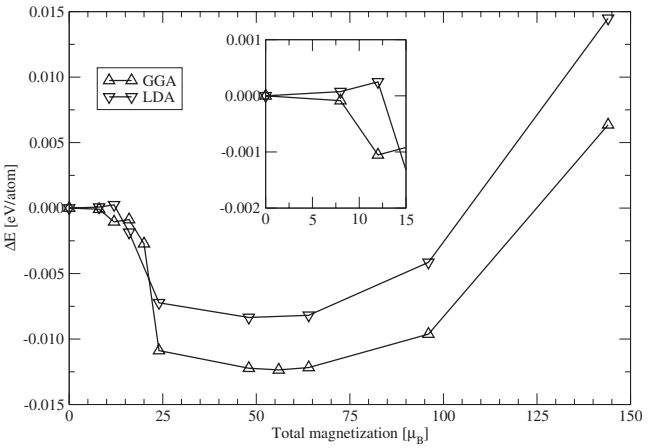

FIG. 1. Total energy of the 2/1 approximant as a function of the total magnetic moment per unit cell as determined by fixed moment calculations. The inset shows the detail of the plot for a small magnetization.

strate that the gain in magnetic energy remains very small up to a total moment of about $M \sim 10\mu_B$ per cell followed by a sharp drop at about $20\mu_B$ and a minimum at a total moment of $M \sim 60\mu_B$. An important difference between the LSDA and the GGA exists for small magnetizations: In the LSDA $M=0$ is a local minimum, the nonmagnetic state is metastable—i.e., if the symmetry-breaking average moment is set initially to a value of $0.2\mu_B$ or less, the calculations converge to the nonmagnetic state. The calculations have to be initialized with a larger average moment to detect the true magnetic ground state. This explains the absence of magnetism in our previous calculations on the 1/1 and 2/1 approximants.[10] In the GGA calculations, the energy of the nonmagnetic state is a local maximum; even if the calculations are initialized with a very small magnetic moment, they will converge to the true magnetic ground state. With a minimum in the magnetic energy at about $M=60\mu_B$/cell and 48 Mn atoms, the average magnetic moment per Mn atom is $1.25\mu_B$, the important question to be answered is not "can magnetic moments exist on Mn atoms in quasicrystals?" but rather "why are most Al-Pd-Mn quasicrystals only weakly magnetic?" This of course includes the question for the topological characterization and the chemical coordination of the Mn sites carrying magnetic moments. To answer these questions requires first a detailed analysis of their quasiperiodic structure.

III. KATZ-GRATIAS-BOUDARD MODEL OF *i*-Al-Pd-Mn QUASICRYSTAL

Icosahedral Al-Pd-Mn belongs to the icosahedral *F*-type (face-centered) quasicrystals. A structural model for this class of quasicrystals was first proposed by Cornier *et al.*[44] as a model for an icosahedral Al-Cu-Fe quasicrystal. In the literature this model is mostly referred to as the model of Katz and Gratias (KG model).[45] The KG model consists of three types of occupation domains (also called atomic surfaces or occupation windows) decorating the vertices of a 6D hypercubic lattice. Boudard *et al.*[46] and de Boissieu *et al.*[47] successfully applied the model to the description of the structure of icosahedral Al-Pd-Mn. They proposed a shell structure of the spherical occupation domains defining the chemical ordering of aluminum and transition-metal atoms. As the spherical shells forming the occupation domains lead to some unacceptably short interatomic distances in real space, we replaced the spherical shells of Boudard *et al.*[46] by triacontahedral ones.[48] We denote this model as the model of Katz-Gratias-Boudard (KGB model).

In the KGB model of *i*-Al-Pd-Mn the lattice nodes in 6D space are decorated by three kinds of triacontahedral occupation domains: a triacontahedron at the "even" nodes n_0 and the "odd" nodes n_1 and a smaller triacontahedron at the body-centered bc_0 positions. The occupation domain at the n_1 node is truncated by its intersections with its 12 images displaced by τ^3 [with the golden mean $\tau=(1+\sqrt{5})/2$] along the fivefold axes. The fivefold radii of the large triacontahedra at n_0 and n_1 are τ and the radius of the smaller one at bc_0 is τ^{-1}. The shell structure of the occupation domains defines the chemical ordering, which has a significant influence on the electronic and magnetic properties of the quasicrystal. The large triacontahedra at the even nodes n_0 and the odd nodes n_1 contain small triacontahedra in the center occupied by Mn atoms. At the n_0 node the Mn core is surrounded by an outer Al shell. At the even node n_1 the Mn core is surrounded by an inner Pd shell and an outer Al shell. In our version of the KGB model the radii of the inner shells containing transition-metal atoms are τ^{-1} at n_0 and $2\tau^{-1}$ and $2\tau^{-2}$ at n_1. The body-centered bc_0 positions are occupied by Pd atoms only.

In any numerical calculation one has to work with finite models. The introduction of a linear phason strain allows to construct a sequence of approximants of different sizes. The approximants are labeled by Fibonacci numbers as F_{n+1}/F_n, where $n=1,2,\ldots$. The 1/1 approximant to *i*-Al-Pd-Mn has 128 atoms/cell, the 2/1, 3/2, and 5/3 approximants have 544, 2920, and 9700 atoms/cell, respectively. The 6D lattice points projected onto the perpendicular space form a cubic mesh. Because of periodicity of the approximants the triacontahedral shape of the domains of an infinitely extended quasicrystal is replaced by a coarse-grained approximation, see Fig. 2. The occupation domains can be decomposed into cubic grains. The size Δ of the grain is equal to $\Delta=\tau^2/\sqrt{\tau+2}/F_{n+3}$. The grains are thus rather coarse for small approximants but become finer with increasing order of the approximant. For instance, a diameter of the n_0 (or n_1) occupation domain measured along a twofold direction is for a F_{n+1}/F_n approximant equal to $2F_{n+3}\Delta$. Vertices of the 6D lattice with the even (odd) parity are projected into the grains with the same parity. Therefore only half of the grains (mesh points) in the occupation domains correspond to atomic sites, see Fig. 2. The occupation domains in our KGB model are centered with respect to the cubic mesh in the body-centered (0.5,0.5,0.5) position. With this choice the space-group symmetry is $P2_13$ (No. 198) for all approximants. We note that in this case there are no mesh points in the centers of the occupation domains. An alternative choice centered at the (0,0,0) position leads to a $Pm3$ symmetry of the approximants; but this choice leads to ambiguities when the mesh points fall on the surface of the occupation domains. To center of the oc-

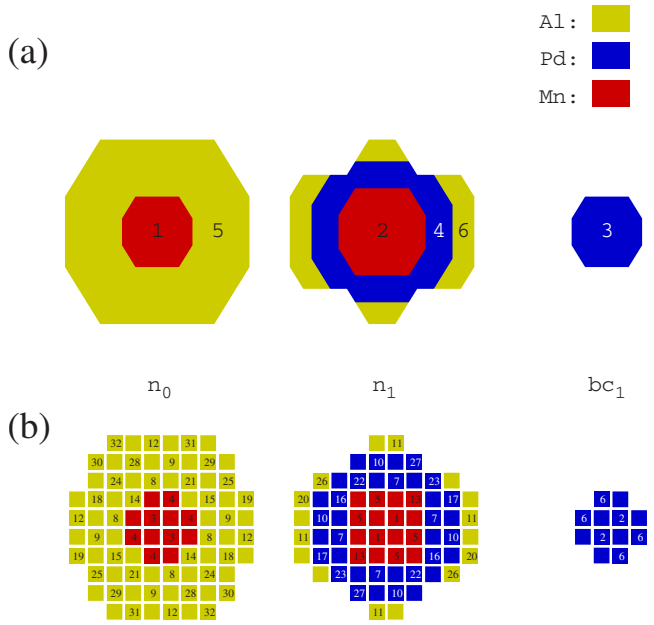

FIG. 2. (Color online) (a) A cut through the occupation domains of the KGB model of quasicrystalline *i*-Al-Pd-Mn in perpendicular space. The internal shell structure of the occupation domains determines the chemical identity of atoms. The shells are labeled by shell indices S, with $S=1,2,\ldots,6$. (b) Cut through the occupation domains for the 2/1 approximant. Because of the periodicity of the approximant the triacontahedral shape of the domains of a quasicrystal is replaced by a coarse-grained approximation. The inscribed numbers refer to the atomic orbits, see Table I.

cupation domains at high-symmetry points has computational advantages. (i) The Brillouin zone has a point-group symmetry that allows us to reduce the number of $\vec{k}$ points. (ii) The structure can be expressed in terms of rather small number of atomic orbits (Wyckoff positions) with multiplicities 12 or 4. This simplifies the discussion of chemical ordering. The atomic positions in an orbit are equivalent; they have the same environments, the same local densities of states, and the same magnetic polarization. This makes it possible, for instance, to explore the effect of small changes in the environment of Mn atoms on their magnetic moments, induced by a small distortion of the perfect point-group symmetry.

A. Structural model of 2/1 approximant

All our studies of the electronic and magnetic properties of *i*-Al-Pd-Mn were performed on a 2/1 approximant. The 2/1 approximant consists of 544 atoms in a cubic unit cell. The next approximant with 2920 atoms per unit cell is already too large for *ab initio* DFT studies. The edge of the unit cell of the 2/1 approximant is $2a_{qc}\tau^3/\sqrt{\tau+2}=20.31$ Å, with the quasilattice constant $a_{qc}=4.56$ Å. Table I collects the structural data of the models used in our calculations. Each atomic position is described, in addition to the x, y, and z coordinates in real space by its image in perpendicular space given by the three indices h, k, and l. As the occupation domain is centered at the (0.5,0.5,0.5) position the positions of the atoms with respect to the center of the occupation domain are $h-0.5$, $k-0.5$, and $l-0.5$. Figure 2(b) shows a cut through the occupation domains at $l=1$. The internal shell structure of the occupation domains determines the chemical decorations of the sites. The shells are labeled by shell indices S, where $S=1,2,\ldots,6$. To each shell a chemical species is assigned according to the rule: $(1,2)\rightarrow$Mn, $(3,4)\rightarrow$Pd, and $(5,6)\rightarrow$Al. Because of the point-group symmetry the positions can be grouped into orbits with multiplicity 12 (a general position) or 4 (a position on the body diagonal). The 2/1 approximant has 50 inequivalent orbits. A list of all atomic orbits, with their Cartesian coordinates x, y, and z, the indices h, k, and l of their images in perpendicular space, and the shell indices defining the chemical decoration, is given in Table I.

In our study we have considered several chemical variants of the 2/1 approximant. The diversity of the chemical ordering allows us to distinguish different mechanisms contributing to the formation of magnetic moments on Mn atoms. The chemical variants are labeled by letters $A-F$. The variant A is the reference model. It has the chemical decoration determined by the triacontahedral shape of the shells in the occupation domains. The other variants are modifications of this reference model. We have considered only modifications that affect the shape of the interfaces between the shells. In particular the interface between shells 4 and 6 at node n_1 appears to be significant. In Sec. I we shall demonstrate that a modification of this interface has an essential influence on the magnetic properties and the structural stability of the quasicrystal. Table I lists in columns S_A-S_F the shell indices of all chemical variants. For sake of simplicity in columns S_B-S_F only the assignment of an orbit to a different shell as in the reference model A is listed. Variant B was found to have the lowest structural energy. It differs form the reference model A only in two atomic orbits, 17 and 42. The shell indices of these orbits changed from 4 to 6, i.e., the Pd atoms occupying these sites are replaced by Al. For this model cuts through the occupation domains in perpendicular space are shown in Fig. 3. The chemical variants $C-F$ are used to study of the influence of chemical ordering on the magnetic properties, as presented in Sec. II.

IV. FORMATION OF MAGNETIC MOMENT ON Mn ATOMS

As already mentioned in Sec. I two major mechanisms contribute to the formation of magnetic moments on Mn atoms: (i) loosely packed environments of the Mn atoms and (ii) the interaction of the Mn atoms with nearest-neighbor Pd atoms leading to a shift of the Mn d band to lower binding energies. Both mechanism contribute to the increased local density of states at the Fermi level $n_i(E_F)$ on the Mn_i atom. According to the Stoner criterion a magnetic moment is formed if the paramagnetic DOS $n_i(E_F)$ is higher than certain threshold. In this section both mechanisms are analyzed in detail.

A. Loosely packed Mn environment

A model of the *i*-Al-Pd-Mn quasicrystal with idealized coordinates derived from hyperspace geometry can be used

TABLE I. Structural data of all considered models of the 2/1-Al-Pd-Mn approximants. The first column defines the labels of the atomic orbits, x, y, and z are the relative atomic coordinates in the elementary cell in real space, h, k, and l are the indices in perpendicular space, and the next column is the multiplicity of the atomic orbit. Coordinates of the other atoms in the orbit are obtained by symmetry operations. The S_i, $i=A-F$ label the shells in the occupation domains, see Fig. 1. Letters $A-F$ label the chemical variants considered in our work, model A is the reference model, models $B-F$ are modifications of A generated by reassigning the chemical occupation of certain orbits. Blank values or values marked by "=" mean that the shell index S_x is the same as S_A. Chemical species assigned to the shells are: $(1,2)\rightarrow$Mn, $(3,4)\rightarrow$Pd, and $(5,6)\rightarrow$Al.

No.	x	y	z	h	k	l	Multiplicity	S_A	S_B	S_C	S_D	S_E	S_F
1	−0.1545	−0.1545	−0.1545	1	1	1	4	2					
2	0.3455	0.3455	0.3455	1	1	1	4	3					
3	0.1545	0.1545	0.1545	0	0	0	4	1					
4	0.0365	0.3455	−0.1545	2	1	1	12	1	=	=	=	=	5
5	−0.0365	−0.3455	0.1545	−1	0	0	12	2					
6	0.4635	0.1545	−0.3455	−1	0	0	12	3					
7	0.2275	−0.1545	−0.1545	3	1	1	12	4					
8	−0.2275	0.1545	0.1545	−2	0	0	12	5					
9	0.4184	0.3455	−0.1545	4	1	1	12	5					
10	−0.4184	−0.3455	0.1545	−3	0	0	12	4					
11	−0.3906	−0.1545	−0.1545	5	1	1	12	6					
12	0.3906	0.1545	0.1545	−4	0	0	12	5					
13	0.0365	−0.4635	0.3455	2	2	1	12	2					
14	−0.0365	0.4635	−0.3455	−1	−1	0	12	5					
15	0.2275	0.0365	0.3455	3	2	1	12	5					
16	−0.2275	−0.0365	−0.3455	−2	−1	0	12	4					
17	0.4184	−0.4635	0.3455	4	2	1	12	4	6	6	=	=	=
18	−0.4184	0.4635	−0.3455	−3	−1	0	12	5					
19	−0.3906	0.0365	0.3455	5	2	1	12	5					
20	0.3906	−0.0365	−0.3455	−4	−1	0	12	6					
21	0.0365	−0.2725	−0.1545	2	3	1	12	5					
22	−0.0365	0.2725	0.1545	−1	−2	0	12	4					
23	0.2275	0.2275	−0.1545	3	3	1	12	4					
24	−0.2275	−0.2275	0.1545	−2	−2	0	12	5					
25	0.4184	−0.2725	−0.1545	4	3	1	12	5					
26	−0.4184	0.2725	0.1545	−3	−2	0	12	6					
27	0.0365	−0.0816	0.3455	2	4	1	12	4					
28	−0.0365	0.0816	−0.3455	−1	−3	0	12	5					
29	0.2275	0.4184	0.3455	3	4	1	12	5					
30	−0.4184	0.0816	−0.3455	−3	−3	0	12	5					
31	0.0365	0.1094	−0.1545	2	5	1	12	5					
32	−0.2275	0.3906	0.1545	−2	−4	0	12	5					
33	−0.4635	−0.4635	−0.4635	2	2	2	4	5					
34	0.4635	0.4635	0.4635	−1	−1	−1	4	2	=	=	=	4	=
35	−0.2725	0.0365	−0.4635	3	2	2	12	4					
36	0.2725	−0.0365	0.4635	−2	−1	−1	12	5					
37	−0.0816	−0.4635	−0.4635	4	2	2	12	5					
38	0.0816	0.4635	0.4635	−3	−1	−1	12	6					
39	0.1094	0.0365	−0.4635	5	2	2	12	6					
40	−0.1094	−0.0365	0.4635	−4	−1	−1	12	5					
41	−0.2725	0.2275	0.0365	3	3	2	12	5					
42	0.2725	−0.2275	−0.0365	−2	−2	−1	12	4	6	=	6	=	=
43	−0.0816	−0.2725	0.0365	4	3	2	12	6					

TABLE I. (*Continued.*)

No.	x	y	z	h	k	l	Multiplicity	S_A	S_B	S_C	S_D	S_E	S_F
44	0.0816	0.2725	−0.0365	−3	−2	−1	12	5					
45	−0.2725	0.4184	−0.4635	3	4	2	12	6					
46	0.2725	−0.4184	0.4635	−2	−3	−1	12	5					
47	0.2275	0.2275	0.2275	3	3	3	4	6					
48	−0.2275	−0.2275	−0.2275	−2	−2	−2	4	5					
49	0.4184	−0.2725	0.2275	4	3	3	12	5					
50	−0.4184	0.2725	−0.2275	−3	−2	−2	12	6					

for studies of various physical properties. However, the magnetic moments on the Mn atoms are so sensitive to their local environments that a model with the idealized coordinates is not sufficiently realistic. We shall show that a model of a quasicrystal with the idealized coordinates exhibits unphysically large magnetic moments on Mn atoms.

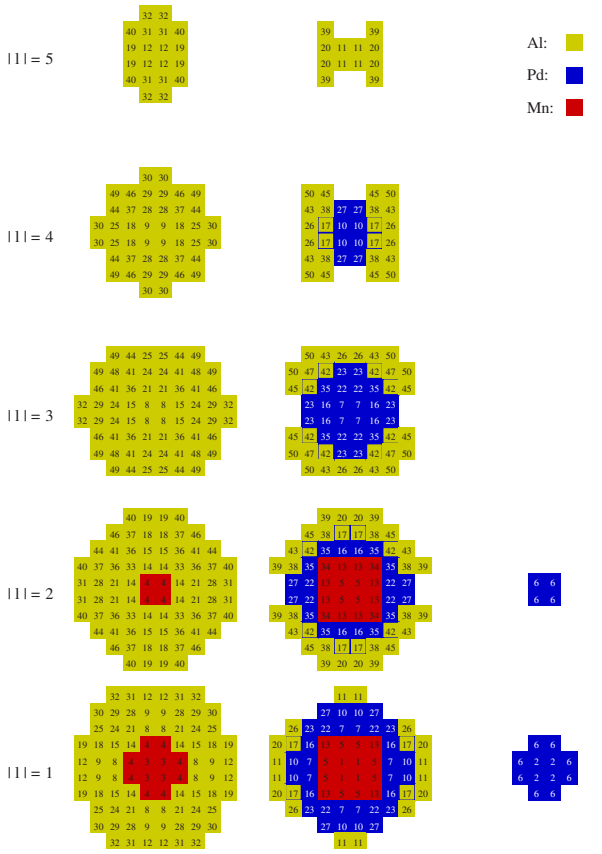

FIG. 3. (Color online) A complete view of the shell structure of the occupation domains in perpendicular space for the energetically most stable and nonmagnetic chemical variant (model *B*). The inscribed numbers refer to the atomic orbits. The coordinates of the corresponding atoms in the real space and other structural data can be found in Table I. The slices of the domains are indexed by $|l|=1,2,\ldots,5$. The slices for $\pm l$ are shown together. The occupation domains of the reference model *A* and model *B* differ in the atomic orbits 17 and 42.

1. Structure with ideal coordinates derived from 6D geometry

The coordinates of atoms in an idealized model are obtained directly by the 6D projection. In model *A* of the 2/1 approximant 48 atoms out of 544 are Mn atoms. A spin-polarized calculation of the electronic structure shows that the majority of Mn atoms exhibit significant magnetic moments; see Fig. 4. Because of the point-group symmetry the Mn atoms are grouped into six atomic orbits 1(4), 13(12), 3(4), 34(4), 4(12), and 5(12) with the multiplicities 4 and 12 given in the brackets. The local environments and hence also the magnetic moments of all atoms in the same atomic orbit are equal.

The calculated high values of magnetic moments contradict experimental observations. Hippert *et al.*[5,49] studied the low-temperature dependence of the magnetic susceptibility in several samples of *i*-Al-Pd-Mn quasicrystals. They concluded that only few Mn atoms carry a localized magnetic. The concentration x_C of magnetic Mn atoms depends on the

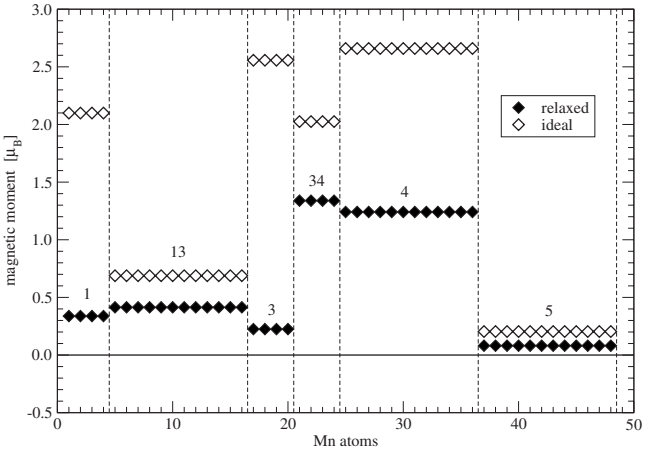

FIG. 4. Comparison of the calculated magnetic moments of Mn atoms in model *A* with ideal coordinates and in the same model with coordinates relaxed by Hellmann-Feynman forces from DFT calculations. In the 2/1 approximant there are 48 Mn atoms. Because of the symmetry they are grouped into orbits with multiplicity 12 or 4 (separated by vertical dashed lines). All atoms in the same orbit have the same environments and hence the same magnetic moment. The numbering of the orbits is shown in Table I. The relaxation leads to more compact atomic environments of the Mn atoms and consequently to a substantial reduction in their magnetic moments.

TABLE II. Fraction x_C of magnetic Mn atoms, calculated according to the prescription of Hippert *et al.* (Ref. 5) (cf. text) and total magnetization density M of different variants of models A and B (ideal, with relaxed coordinates, high-temperature annealed, and quenched after annealing, cf. text). Model B with the relaxed coordinates is essentially nonmagnetic and exhibits the lowest total energy.

Model	Coordinates	x_C (%)	M [10^{-3} $\mu_B/\text{Å}^3$]
A	Ideal	15.3	7.61
A	Relaxed	5.4	4.19
A	Annealed	5.3	3.31
A	Quenched	4.4	2.97
B	Ideal	5.7	2.98
B	Relaxed	0.006	0.39

sample composition and ranges from ≈2.3% for the most magnetic samples down to ≈0.044% for less magnetic samples. The estimate of the concentration of magnetic Mn atoms is based on the value of the Curie constant C which is proportional to $x_C N_{\text{Mn}} S(S+1)$, with N_{Mn} as the total number of Mn atoms in the sample and S equal to $\frac{5}{2}$; assuming that a Mn atom is magnetic, it has the maximal magnetic moment of $5\mu_B$. The subscript in x_C denotes that the fraction has been estimated on the basis of these assumptions.

In a quasicrystal model with idealized coordinates the magnetic moments of the Mn atoms values range from $0.2\mu_B$ to $2.7\mu_B$. If one estimates the fraction of magnetic Mn atoms in this model using the same assumptions as Hippert *et al.*,[5] $x_C=15.3\%$. This value substantially exceeds the experimentally determined upper limit. However, we shall show that the magnetic moments of the Mn atoms depend very sensitively on local environment and chemical ordering and a slight modification of the model can lead to a reduction in the magnetic moments or even to a complete disappearance of magnetism.

2. Structure with relaxed coordinates

The most important factor determining magnetic-moment formation is the interaction of an Mn atom with the neighboring atoms. Distances to nearest neighbors must be determined very accurately. From this point of view in a more realistic model of the quasicrystal the coordinates of all atoms must be in equilibrium with respect to the interatomic forces. Figure 4 presents a comparison of the magnetic moments of Mn atoms in a model of the 2/1 approximant with ideal coordinates and with coordinates relaxed under the Hellmann-Feynman forces from DFT calculations. The relaxation leads to a substantial reduction in all Mn moments. Only Mn atoms from two atomic orbits, 34 and 4 carry a large magnetic moment, $m(34)=1.34\mu_B$ and $m(4)=1.24\mu_B$. The fraction of magnetic Mn atoms calculated according to Hipperts rule is $x_C=5.4\%$, see Table II. This is still higher by a factor of 2 than the upper experimentally determined limit.[5]

The substantial reduction in the magnetic moments in the relaxed state is a consequence of a more compact packing around the Mn atoms. The local electronic density of states of a Mn atom in a loosely packed environment is impurity-like. The d band is narrow, the Fermi level falls on the high peak of the local paramagnetic DOS and favors spin polarization. A loosely packed environment of a Mn atom favors formation of a magnetic moment.

Loose packing occurs in noncrystalline systems (liquid and amorphous) as a consequence of thermal fluctuations. Indeed it has been observed that the paramagnetic susceptibility of molten Al-Pd-Mn exceeds that of quasicrystal. In a quasicrystalline system the ideal coordinates do not reflect the smaller size of Mn atom compared to Al or Pd. Approximately 70% of nearest neighbors of Mn atoms are located in the directions of the threefold symmetry axes at a distance of 2.57 Å, the other are located along the twofold directions at a distance of 2.96 Å. Upon relaxation the Al atoms at a distance 2.96 Å move inwards; see Sec. IV B.

The loosely packed environments in a model with ideal coordinates can be considered as unphysical, as they disappear upon relaxation. However, larger Mn-Al distances are only one possible reason for a loose packing around the Mn atom. The other possibility is a low coordination of the Mn atoms at special sites. In the i-Al-Pd-Mn quasicrystal one obvious candidate for a loosely packed place is the center of the pseudo-Mackay cluster (orbit 4), where the Mn atom has only 7 or 8 nearest neighbors as confirmed by extended x-ray-absorption fine structure (EXAFS) experiment.[50] In the ideal structure these Mn atoms are strongly magnetically polarized [e.g., $m(4)=2.66\mu_B$]. During the relaxation the packing of atoms around the central Mn atoms becomes more compact and their magnetic moments are reduced. In Sec. IV B it will be demonstrated that the origin of magnetic moments on these sites is not a loosely packed environment but the direct Mn-Pd interaction.

3. Thermal disorder

The point-group symmetry of the model allowing to classify the atomic positions into orbits is broken in real systems. One source of disorder is the thermal movement of the atoms. To demonstrate the effect of thermal disorder on the magnetic moments, the model of the 2/1 approximant was annealed at 1200 K using *ab initio* molecular-dynamics (MD) method. At this temperature the system is still below melting, but the temperature is high enough to allow not only vibrational movements but also a modest interdiffusion, particularly of Al atoms. After approximately 400 MD steps equilibration of the potential energy fluctuations was observed. The simulation was extended over 2000 MD steps of 10^{-15} s. We prepared two samples for further calculations. One corresponds to the instantaneous positions of atoms at 1200K, in the second the quasicrystal was quenched to 0 K using a conjugated-gradients algorithm. The atoms in the quenched sample relax into nearest force-free positions.

Figure 5 shows the distribution of the magnetic moments of the Mn atoms in a high-temperature annealed quasicrystal. It demonstrates the effect of thermal disorder on magnetic moments. The magnetic moments of individual Mn atoms exhibit considerable scatter which is only slightly reduced after quenching to $T=0$ K. It is interesting to observe that

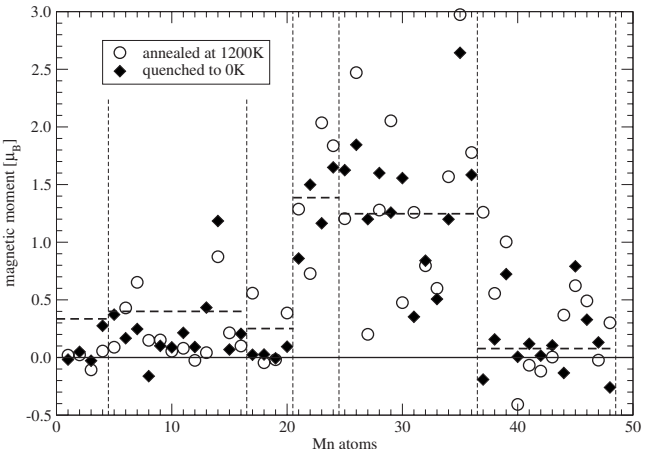

FIG. 5. The effect of thermal disorder on the magnetic moments of Mn atoms in model *A*. Open circles represent magnetic moments calculated for instantaneous positions of atoms at 1200 K. Diamonds show the magnetic moments after a total-energy minimization at $T=0$ K. Vertical dashed lines separates atomic orbits, and horizontal dashed lines indicate the value of magnetic moment for the relaxed system, cf. Fig. 4.

even the moments calculated for a instantaneous high-T configuration reflects the classification into atomic orbits, emphasizing the importance of the local chemical order (which is hardly affected by the annealing). The magnetic polarization expressed as a fraction of Mn in the annealed and quenched systems is $x_C=5.3\%$ and $x_C=4.4\%$, respectively; see Table II. The higher value of the magnetization is almost independent with respect to the statically relaxed configuration. The slightly reduced value found after quenching to $T=0$ K shows that high-T annealing and quenching achieve a more compact configuration.

B. Mn-Pd interaction

The results discussed so far suggest that the major factor influencing the formation of a magnetic moment on Mn atoms is the chemical identity of its neighbors. It is well known that the direct Mn-Mn exchange interaction strongly supports the formation of magnetic moments on neighboring Mn atoms. In the KGB model of *i*-Al-Pd-Mn Mn atoms are separated by a distance at least 4.5 Å. Of course, an indirect interaction between Mn atoms may also play an important role. This point is discussed in Sec. V.

Already in our previous work[16] we concluded that the presence of Pd atoms in the first neighbor shell of an Mn atom has substantial influence on formation of its magnetic moment. This observation was also confirmed by a recent study of Godonyuk *et al.*[51]

Figure 6 shows the dependence of the magnetic moments of the Mn atoms in the ideal and relaxed models on the number of Pd atoms in their nearest-neighbor shell. After relaxation only Mn atoms from atomic orbit 4 with 2 Pd neighbors or from the atomic orbit 34 with 3 Pd neighbors conserve a large magnetic moment. Magnetic moments of other Mn atoms are smaller than $0.5\mu_B$. Figure 7 shows the dependence of the magnetic moments on the number of Pd

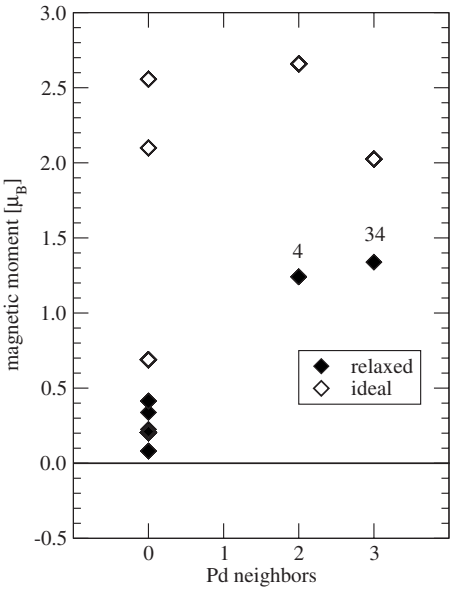

FIG. 6. Magnetic moments of Mn atoms in the ideal and relaxed model *A* in dependence on the number of Pd atoms in their nearest-neighbor shell. After relaxation only the Mn atoms from the atomic orbit 4 with two Pd neighbors or from the atomic orbit 34 with three Pd neighbors conserve a magnetic moment larger than $0.5\mu_B$.

neighbors for the quenched model. The scatter of the magnetic moments for Mn atoms with 2 or 3 Pd neighbors is not surprising. Magnetic moments larger than $0.5\mu_B$ appear also on Mn atoms with no Pd neighbors. The origin of these moments can be attributed to quenched loosely packed environments.

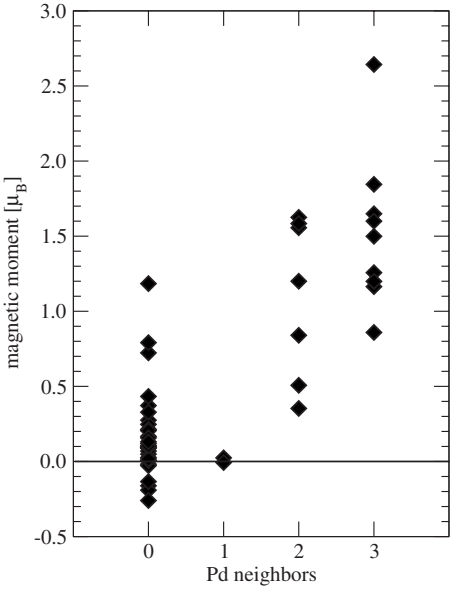

FIG. 7. Dependence of the magnetic moments of Mn atoms on the number of Pd neighbors for the quenched model *A*. The scatter of magnetic moments for Mn atoms with two or three Pd neighbors is not surprising. Magnetic moments larger than $0.5\mu_B$ appear also on Mn atoms with no Pd neighbors. The origin of these moments can be attributed to quenched defects with loosely packed environments.

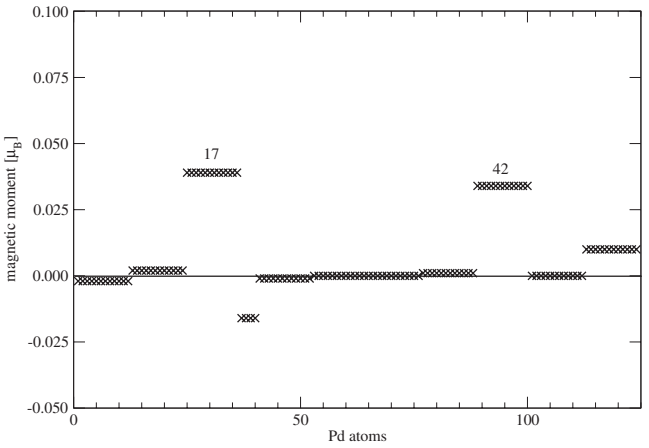

FIG. 8. If Pd atoms are in a close contact with a magnetic atom they can also become partially magnetically polarized. The figure shows the magnetic polarization of Pd atoms in model *A* containing 124 Pd atoms grouped in 11 atomic orbits. While the magnetic polarization of the majority of the Pd atoms is very small, Pd atoms from the atomic orbits 17 and 42 which are nearest neighbors to Mn atoms carry non-negligible magnetic moments.

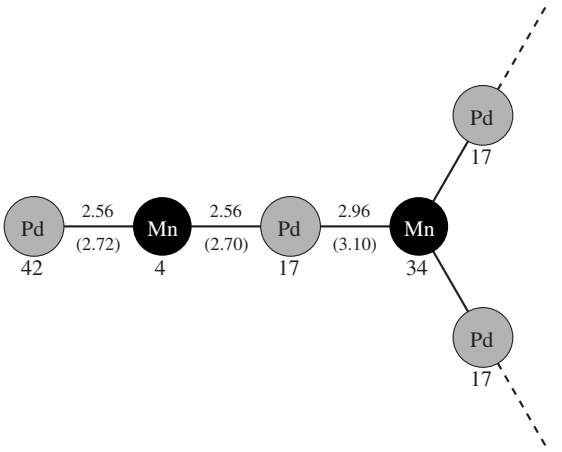

FIG. 9. Bonding around the magnetically polarized Mn atoms from the atomic orbits 4 and 34. The Mn(4) atoms have two Pd neighbors, Pd(42) and Pd(17). In a model with ideal coordinates both Pd atoms are located at a distance 2.56 Å from the central Mn atom. After relaxation the interatomic Mn-Pd distance increases to 2.70 and 2.72 Å for Pd(17) and Pd(42) atoms, respectively. The Mn(34) atom is located at the body diagonal of the model and it has a threefold symmetry. Three Pd(17) neighbors are located at a distance 2.96 Å which after relaxation increases to 3.1 Å. The increase in the interatomic Mn-Pd distances reflects the repulsive Mn-Pd interaction.

The interaction of a Mn atom with Pd atoms in its first neighbor shell contributes to the formation of a magnetic moment on the Mn atom. The explanation of this mechanism is straightforward. The Mn *d* band is always located close to the Fermi level. The *d* band of Pd is located at higher binding energies with a peak around −4 eV. The Mn-Pd interaction is repulsive, the *d* bands of Pd and Mn atoms repel each other, leading to a shift of the Mn *d* band to lower binding energies. The local Mn *d* DOS at the Fermi level increases with the shift of the *d* band. According to the Stoner criterion a magnetic moment is formed if the paramagnetic DOS is higher than certain threshold. Mn atoms with two or more Pd atoms in the first neighbor shell are magnetically polarized. On the other hand, Fig. 7 demonstrates that one Pd atom in the first neighbor shell only is not sufficient to induce a magnetic moment on the Mn atom.

Hence the direct Mn-Pd interaction contributes to the formation of magnetic moments on the Mn atoms independently of the existence of the loosely packed environments. As this mechanism is essential for the understanding of the origin of magnetism in *i*-Al-Pd-Mn quasicrystals it deserves a more detailed analysis.

1. Nonmagnetic ground state

Pd is considered as a nonmagnetic element. Nevertheless, if Pd atoms are in close contact with a magnetic atom, an induced magnetic moment can be formed. In Fig. 8 the magnetic moments of Pd atoms in the 2/1 approximant are presented. In this model there are 124 Pd atoms grouped in 11 atomic orbits. Here we present the results for the model with relaxed atomic positions only. While the magnetic polarization of the majority of the Pd atoms is negligibly small, atoms from orbit 17 carry a moment of $0.039\mu_B$ and those from orbit 42 have a moment of $0.034\mu_B$. These atoms are nearest neighbors to the Mn atoms with the largest moments.

Figure 9 sketches the Mn-Pd bonds around the magnetically polarized Mn atoms from the atomic orbits 4 and 34. Mn(4) atoms have two Pd neighbors, Pd(42) and Pd(17). Both Mn(4) and Mn(34) sites occupy the centers of the pseudo-Mackay clusters. In a model with ideal coordinates both Pd atoms are at a distance of 2.56 Å from the central Mn atom. Upon relaxation the Mn-Pd distance increases to 2.70 and 2.72 Å for Pd(17) and Pd(42) atoms, respectively. Mn(34) atoms are located along the body diagonal of the unit cell, these sites have threefold symmetry. Three Pd(17) neighbors located at a distance 2.96 Å, which upon relaxation increases to 3.1 Å.

We note that the atomic orbit 34 has multiplicity 4, therefore there are four such Mn-Pd configurations in the 2/1 approximant as presented. In the 2/1 approximant Mn atoms with two Pd neighbors and Mn atoms with three Pd neighbors form a Mn-Pd cluster. We have analyzed the topology of Mn-Pd bonding also in higher approximants up to the 21/13 approximant and found that in all these models Mn atoms with 2 or 3 Pd neighbors exist. Part of them are also clustered into configurations similar to that in Fig. 9. The origin of existence of the Mn-Pd neighbors in the *i*-Al-Pd-Mn quasicrystal is discussed more in detail in Sec. IV C.

To demonstrate that the direct Mn-Pd interaction is dominant for an appearance of magnetism in *i*-Al-Pd-Mn quasicrystals, we have prepared several modified models. In model *B* we replaced the Pd(17) and Pd(42) atoms by Al atoms, hence no Mn atom has a Pd neighbor. Figure 10 compares magnetic moments of Mn atoms in model *B* with ideal and with relaxed coordinates. In the model with ideal coordinates the magnetic moments of Mn atoms form orbits 1, 3, and 13 remain essentially the same as in the idealized model *A*, see also Fig. 4. The magnetic moment of Mn(5) atoms increases

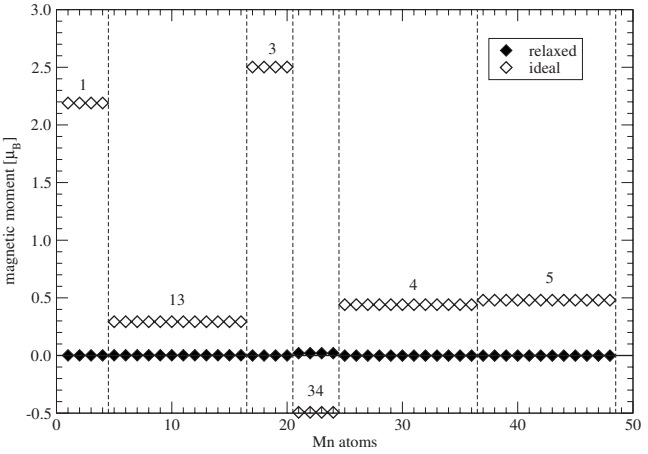

FIG. 10. Comparison of the magnetic moments of Mn atoms in model *B* with ideal and relaxed coordinates. In the model with ideal coordinates the magnetic moments of Mn atoms remain essentially the same as in the model *A*, compare with Fig. 4, with exception of the Mn atoms from orbits 34 and 4 that have different local environments in model *B*. The most significant result is the fact that in the model *B* with relaxed coordinate magnetism disappears completely. Magnetic moments of all its 48 Mn atoms are essentially zero.

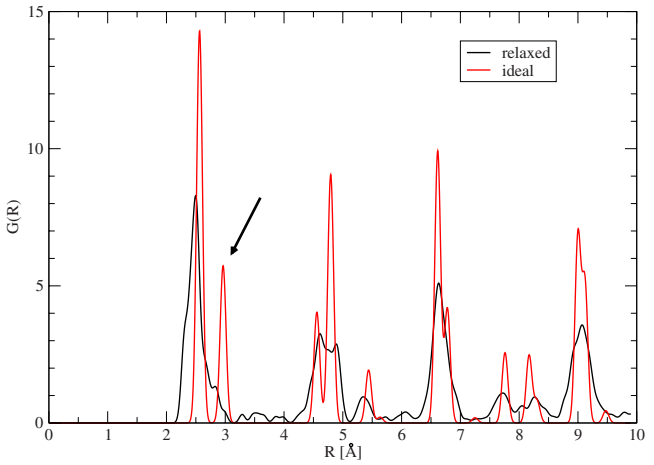

FIG. 11. (Color online) Comparison of the partial Mn-Al pair-distribution function of model *B* with ideal (red/gray lines) and relaxed (black lines) coordinates. While in the model with ideal coordinates Al nearest neighbors are found at two separate distances of 2.56 and 2.96 Å, in the relaxed model Al atoms move closer to the central Mn and the peak at 2.96 Å (marked by an arrow) merges with the first peak. This demonstrates that environment of Mn atoms in the model with ideal coordinates is indeed loosely packed.

from $0.2\mu_B$ to $0.48\mu_B$, but the most important change is observed on sites Mn(4) and Mn(34) where Pd neighbors have been replaced by Al atoms. The magnetic moment of Mn(4) decreases from $2.66\mu_B$ to $0.44\mu_B$, the magnetic moment on Mn(34) sites is even reversed: form $2.03\mu_B$ in model *A* to $-0.49\mu_B$ in the model *B*. This indicates that whereas the indirect Mn-Pd-Mn exchange interaction mediated by *d* electrons is ferromagnetic, the indirect Mn-Al-Mn exchange interaction mediated by the Al *s* electrons is antiferromagnetic, as it will be discussed in Sec. V. In model *B* with the relaxed coordinates magnetism has completely disappeared. The magnetic moments of all 48 Mn atoms are essentially zero, the largest moment of $0.02\mu_B$ is localized on the Mn(34) atoms.

Large magnetic moments in the model with ideal coordinates and their complete disappearance in the model with relaxed coordinates clearly demonstrates that the mechanism driving the formation of the magnetic moments on Mn atoms is their loosely packed environment, as discussed in Sec. IV A. Figure 11 compares the partial Al-Mn pair-distribution function (PDF) of model *B* with ideal and relaxed coordinates. While in the model with ideal coordinates Mn-Al nearest neighbors are at distances of 2.56 and 2.96 Å, in the relaxed model the Mn-Al pair-distribution function shows a single broad peak with a maximum at 2.5 Å, while the partial Mn-Al coordination number remains the same.

Together with the results for the ideal and relaxed model *A* this demonstrates that the origin of magnetic moments on Mn atoms is loosely packed environments. This is true for all Mn atoms except those belonging to orbits 34 ad 4 where the formation of their large magnetic moments is further supported by the Mn-Pd interaction leading to the *d*-band repulsion.

The energetic stability of all models can be characterized by the energy difference ΔE relative to the tie plane defined by the heats of formation of the three binary crystalline intermetallic compounds Al_6Mn, $Al_{11}Mn_4$, and δ-Al_3Pd_2, as calculated (also using VASP) by Mihalkovič and Widom; see Ref. 52. The nonmagnetic model *B* has the lowest energy. The positive structural energy difference of the quasicrystal relative to the crystalline compounds of model *A*, $\Delta E = 78.9$ meV/atom, is decreased in model *B* to $\Delta E = 28.4$ meV; see Table III. Within all models investigated in our study, this model represents the ground state. Hence the ground state of the *i*-Al-Pd-Mn quasicrystal thus seems to be nonmagnetic.

2. Influence of chemical short-range order

In this section we analyze the influence of the chemical identity of neighboring atoms on the magnetic moments on the Mn atoms. From now we consider only models with relaxed coordinates.

Figure 12(a) shows the local *d* DOS on Mn(4) atoms in models *A* and *B*, both with relaxed coordinates. The comparison shows the shift of the *d* states on atom Mn(4) in model *A* toward the Fermi level. In model *B* where the Mn(4) atoms have no Pd neighbors the Fermi levels falls close to the minimum in the DOS created by the bonding-antibonding splitting of the *d* band. In model *A* where the Mn(4) atoms interact with 2 Pd neighbors the Fermi level is located close to the maximum of *d*-band peak due to a *d*-band shift of ≈ 0.5 eV.

In model *A* the origin of the large magnetic moments of Mn atoms belonging to orbits 4 and 34 is the Mn-Pd interaction. To demonstrate how this mechanism works we have prepared further models with chemically modified environments of these Mn atoms.

In model *C* we replace all Pd(17) atoms by Al atoms, now Mn(4) has only one Pd neighbor. Mn(34) atoms have no Pd

TABLE III. Structural, energetic, and magnetic properties of different chemical variants of the 2/1 approximant to the Katz-Gratias-Boudard model of *i*-Al-Pd-Mn. Change in chemical decoration of atomic orbits with respect to the reference model *A* and composition (in atomic percents). The energetic stability of the models is characterized by energy differences ΔE_i (idealized model) and ΔE (relaxed model) above the tie plane defined by heats of formation of binary intermetallic compounds, cf. text. Magnetic properties are given in terms of the average magnetic moment of the Mn atom, $\bar{m}$, and the maximal magnetic moment $m_{\max}$.

Model	Changed atomic orbits	c_{Al}	c_{Pd}	c_{Mn}	ΔE_i (meV/atom)	ΔE (meV/atom)	$\bar{m}$ (μ_B)	$m_{\max}$ (μ_B)	Comment
A		68.4	22.8	8.8	219.0	78.9	0.767	$m(\mathrm{Mn}_{34})=1.51$	Ref. model, magnetic
B	17:Pd→Al 42:Pd→Al	72.8	18.4	8.8	181.4	28.4	0.002	$m(\mathrm{Mn}_{34})=0.02$	Nonmagnetic, lowest energy, no Mn atom has a Pd neighbor
C	17:Pd→Al	70.6	20.6	8.8	189.2	46.6	0.074	$m(\mathrm{Mn}_3)=0.36$	Low magnetization, no Mn atom has more than 1 Pd neighbor
D	42:Pd→Al	70.6	20.6	8.8	205.3	52.5	0.402	$m(\mathrm{Mn}_{34})=2.04$	Mn_{34} has 3 Pd neighbors
E	34:Mn→Pd	68.4	23.5	8.1	216.4	73.0	0.713	$m(\mathrm{Mn}_4)=1.24$	Mn_4 has 2 Pd neighbors
F	4:Mn→Al	70.6	22.8	6.6	194.3	54.9	0.074	$m(\mathrm{Mn}_{34})=0.59$	Mn_{34} has 3 Pd neighbors

neighbors (see Fig. 9). The magnetic moments of Mn atoms are presented in Fig. 13. It has been already observed (see Fig. 7) that one Pd neighbor is not enough to enforce the formation of a magnetic moment on the Mn atom, hence Mn(4) atoms are essentially nonmagnetic, and as expected the magnetic moments of Mn(34) are also negligible.

In model *D* we replaced the Pd(42) atoms by Al atoms, such that only Mn(34) atoms have three Pd neighbors, while Mn(4) atoms have only one. Figure 13 shows that magnetic moments of the Mn(34) atoms exceed $2\mu_B$, while the Mn(4) atoms have only a small magnetic moment of $0.27\mu_B$.

In the next two variants the magnetic Mn atoms were replaced by a nonmagnetic element. In model *E* the Mn(34) atoms are replaced by Pd. Mn(4) atoms have 2 Pd neighbors. Figure 14 confirms that only these atoms have a large moment of $1.24\mu_B$, while the magnetic moments of all other Mn atoms are small but not negligible. We assume that these small moments can be explained by the interaction of Mn atoms with other atoms over distances larger than the nearest-neighbor shell.

In model *F* the Mn(4) atoms are replaced by Al. The magnetic moments of all Mn atoms are essentially zero, except Mn(34) with a moment of $0.59\mu_B$, see Fig. 14. The origin of this moment can be attributed to the direct interaction of the Mn(34) atoms with their three Pd neighbors.

3. Stoner mechanism

Figure 15 presents the local *d* DOS of Mn atoms in the relaxed models *E* and *F*. For model *E* one observes that the *d* states of the Mn(4) atoms with the largest magnetic moment is, similarly as shown in Fig. 12, shifted toward lower binding energies such that the Fermi level falls near the maximum of the *d* band located at ≈ -0.5 eV. The *d* DOS of all other Mn atoms with only a small magnetic moments are broader with maxima around −1.0 eV or even lower. In model *F* the Fermi level falls close to the bonding-antibonding minimum in all DOS's [except Mn(34)] and hence the DOS at Fermi level is small. For Mn(34) the Fermi level is located close to the peak of the local DOS. Comparing the local *d* DOS in models *E* and *F* we see that in model *E* the local *d* DOS of atoms Mn(1), Mn(13), Mn(3), and Mn(5) is substantially enhanced in the region around the Fermi level to value of $n(E_F)\approx 2$ states/eV, i.e., larger than or close to the minimum nonmagnetic DOS required for moment formation according to the Stoner criterion.

Figure 16 shows the correlation between the local paramagnetic DOS at the Fermi level $n(E_F)$ and the magnetic moments on Mn atoms. This analysis confirms that moment formation in *i*-Al-Pd-Mn is driven by a Stoner mechanism. If the paramagnetic DOS at the Fermi level $n(E_F)$ is larger than certain threshold (≈ 2 states/eV/atom) the local paramagnetic susceptibility of the interacting electron system, $\chi=\chi_0/[1-In(E_F)]$ diverges and a local moment is formed. The threshold value of $n(E_F)$ depends on the strength of the Stoner parameter *I* given by exchange splitting divided by the local magnetic moment, $I_i=\Delta E_i/m_i$.

Figure 17 analyzes the relation between the local moment and the exchange splitting of the *d* bands, defined as the difference between the centers of gravity of the bands for the up and down polarizations. The correlation is strictly linear for both the idealized and relaxed models, the slope of the line yields a value of the Stoner parameter of $I=0.75$ eV/μ_B and hence a minimum value of the paramagnetic local density of states of $n(E_F)\approx 1.33$ states/eV for the formation of a local magnetic moment, in agreement with the trend shown in Fig. 16.

C. Origin of magnetism in *i*-Al-Pd-Mn

In Secs. I and III we have identified and described two mechanisms contributing to the formation of magnetic moments on the Mn atoms in *i*-Al-Pd-Mn. In our models the Mn atoms are located in the centers of the pseudo-Mackay clusters. These atoms have a low coordination number (as confirmed by EXAFS experiments[50]) so that the loosely packed environments of these atoms may be considered as responsible for their magnetic moment. However, the analysis of our results for the model *B* show that this is not sufficient. Although these sites are magnetic in a structure based on idealized coordinates, after structural relaxation all manga-

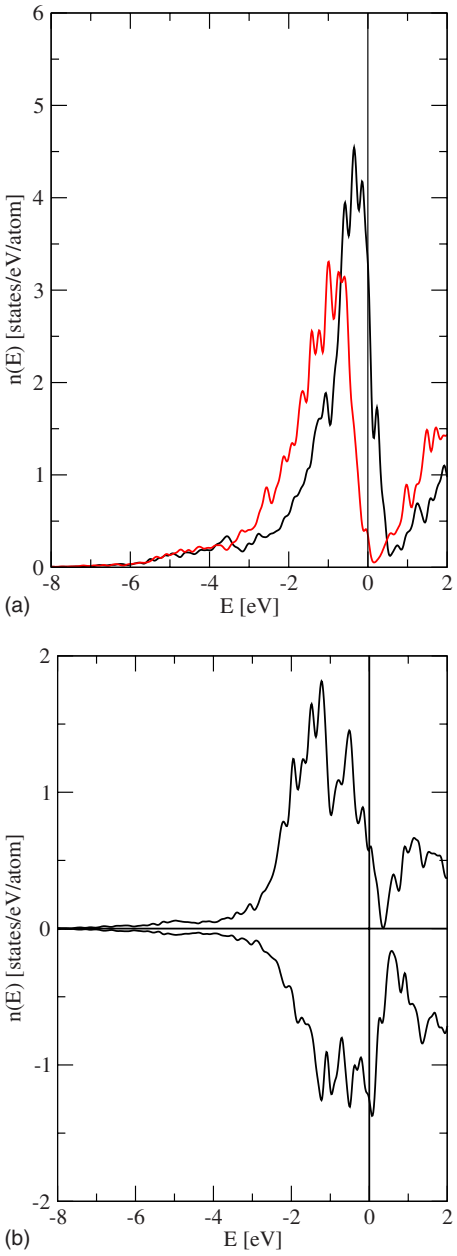

FIG. 12. (Color online) (a) Local *d* DOS on the Mn(4) atoms in models *A* (black line) and *B* (red/gray line), both with relaxed coordinates. The comparison shows the shift of the *d* states on atom Mn(4) toward the Fermi level. In model *B* where Mn(4) atoms have no Pd neighbors the Fermi levels falls close to the minimum in the DOS created by the bonding-antibonding splitting of the *d* states. In model *A* where the Mn(4) atoms interact with two Pd neighbors the *d* states are shifted to lower binding energies such that the Fermi level is located close to the maximum of *d* band peak. (b) Spin-polarized local *d* DOS on the Mn(4) atoms in model *A*.

nese magnetic moments disappeared. In the relaxed model *A* large magnetic moments exist only on those atoms in the centers of the pseudo-Mackay clusters that have at least two or three Pb nearest neighbors. Hence the crucial question is under which circumstances Pd atoms can occupy sites on the first coordination shell of a pseudo-Mackay cluster.

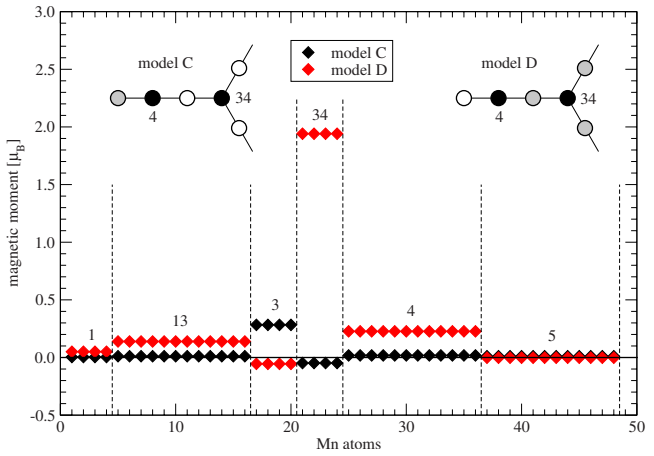

FIG. 13. (Color online) *C* (Black symbols) and *D* (red/gray symbols). The insets illustrate the differences in the local chemical coordination: Mn atoms are shown in black, Pd atoms in gray, and Al atoms as white circles, cf. text.

The atomic structure of *i*-Al-Pd-Mn can be interpreted as a three-dimensional Penrose tiling with the vertices decorated by Bergman and pseudo-Mackay clusters.[53,54] The Bergman and the pseudo-Mackay clusters can be linked along the fivefold or threefold axes. When they are connected along the fivefold direction they share a pentagonal facet. The KGB model predicts that the vertices of this facet are decorated by Pd atoms and that the center of the face is occupied by an Al atom. As the topology and the chemical decoration of the facet required by the building principles for the Bergman cluster is the same as for the pseudo-Mackay cluster, there is no conflict in the site occupation.

However, when the Bergman and pseudo-Mackay clusters are linked along the threefold axis they intersect.[54] An outer part of a Bergman cluster is shared with a pseudo-Mackay cluster and vice versa. This overlap of the clusters leads to a conflict between the chemical decorations required by their building principles, causing the formation of substitutional defects or vacancies. We have identified that just this is the

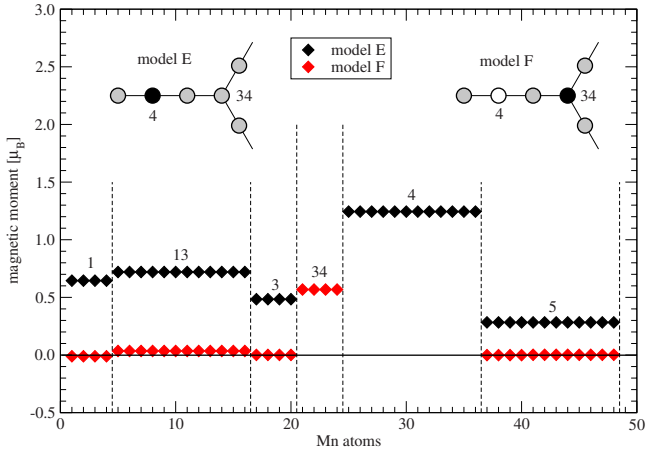

FIG. 14. (Color online) Magnetic moments of Mn atoms in the relaxed models *E* (black symbols) and *F* (red/gray symbols), cf. text. The inset describes the local coordination around atoms belonging to orbits 4 and 34, cf. Fig. 13.

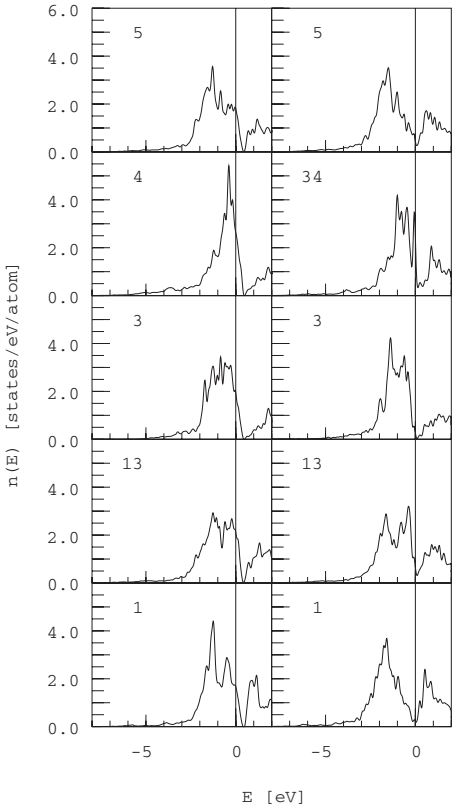

FIG. 15. Paramagnetic local densities of *d* states on Mn atoms in the relaxed models *E* (left column) and *F* (right column), cf. text.

region in the structure responsible for magnetism in the *i*-Al-Pd-Mn quasicrystal.

While according to the building principle of the pseudo-Mackay cluster Al atoms occupy the inner shell of the pseudo-Mackay cluster, the building principle of the Bergman cluster requires a Pd atom at the same position. The conflict between the Bergman and the pseudo-Mackay clusters linked along the threefold axis can be seen in a plane perpendicular to the fivefold axis and eventually even be observed at the fivefold surface of *i*-Al-Pd-Mn.

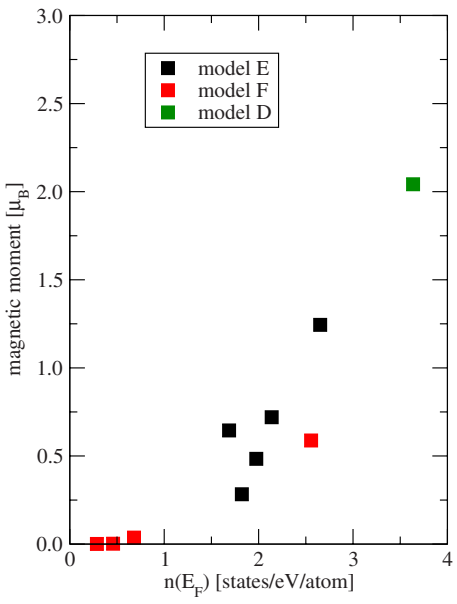

FIG. 16. (Color online) Correlation between the local magnetic moments and the local DOS at Mn sites as calculated for models *D* (green), *E* (black), and *F* (red symbols), all relaxed, cf. text.

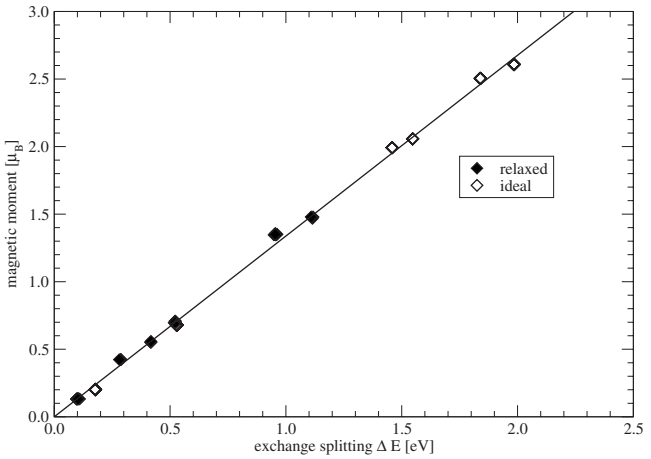

FIG. 17. Magnetic moments versus exchange splitting of the local *d*-band DOS at Mn sites as calculated for the idealized and relaxed model *A*. The slope of the linear fit defines the value of the Stoner parameter *I*, cf. text.

This plane cuts the pseudo-Mackay clusters at the equatorial plane.[55] Figure 18 shows the intersection of the pseudo-Mackay and the Bergman clusters seen along the fivefold axis. The atoms belong to three different layers. The atoms in the top layer are displayed as largest circles. Around the center of the pseudo-Mackay cluster occupied by Mn they form a decagonal ring of Al atoms which is part of the outer shell forming an icosidodecahedron. The center of the Bergman cluster is a Pd atom located 1.26 Å below the top layer. The straight line connecting the centers of the clusters is a threefold symmetry axis. The angle of this axis with the fivefold plane is 10.81°. From the side of the Bergman cluster we see in the top layer a pentagon of Al atoms. One edge of the pentagon (length 2.96 Å) is shared with an edge of the

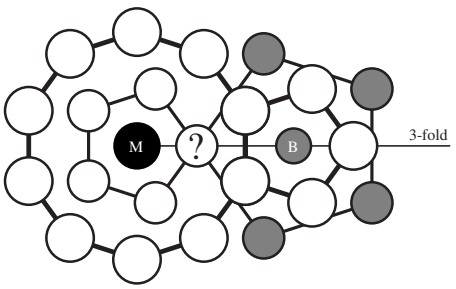

FIG. 18. Schematic representation of the interpenetrating pseudo-Mackay (*m*) and Bergman (*b*) clusters connected along the threefold direction. The black circle represents the Mn(4) atom in the center of the *M* cluster, gray circles Pd atoms in the center and in the second coordination shell of the *B* cluster, and white circles represent Al atoms in both clusters. Large circles represent atoms in the topmost layer and smaller circles atoms in deeper layers. The circle with the question mark is site 17 which can be occupied by a Pd atom (model *A*) or an Al atom (model *B*), cf. text.

decagonal ring. In the top plane there is no conflict between the building principles of the pseudo-Mackay and the Bergman clusters. However, in the second layer which is located 0.48 Å below the top plane the situation is different. The positions of atoms in this second plane are shown as circles of medium size. From the side of the pseudo-Mackay cluster these atoms are Al atoms and belong to the first neighbor shell of the central Mn atom. The positions of these atoms are shown as a small pentagon concentric with the outer decagonal ring. As these sites belonging to the incomplete dodecagonal shell around the center of the pseudo-Mackay cluster not all sites of this pentagon are occupied.

From the side of the Bergman cluster the atoms in this layer also form a pentagon. The edge length of this pentagon is 7.78 Å, and its vertices are decorated by Pd atoms. One vertex of this large pentagon belonging to the Bergman cluster is shared with the small pentagon belonging to the pseudo-Mackay cluster. This vertex is the point of the conflict. From the side of the pseudo-Mackay cluster this site should be occupied by an Al atom, the building principle of the Bergman cluster requires here a Pd atom.

One can speculate which building principle is stronger or which cluster is more stable. Gratias *et al.*[54] based on their structural analysis concluded that the Bergman clusters are the dominant elements of the structure. A similar statement can be found also in the work of Quandt and Elser.[56] Although we agree that the concept of the Bergman clusters is indeed very helpful for the structural analysis, this does not uniquely define the chemical identity of the atoms in the overlapping region.

The KGB model with triacontahedral inner shells of the occupation domains (model *A*) predicts a Pd atom in this site. Gratias *et al.*[54] showed that a pseudo-Mackay cluster can be linked simultaneously with 0–3 different Bergman clusters. A majority of 76.39% of the pseudo-Mackay clusters are linked with two Bergman clusters.[54] The central Mn atom of the pseudo-Mackay cluster thus has in most cases two Pd neighbors. In Secs. I and III we have demonstrated that a Mn atom with 2 Pd neighbors becomes magnetic. On the other hand Pd atoms in these conflicting sites are energetically not favored. Although the formation of magnetic moments on the Mn atoms is accompanied by a decrease in the total energy in comparison with the paramagnetic state, the repulsive interaction between Mn and Pd atoms overbalances this contribution. Model *B* where only Al atoms occupy the conflicting sites is thus by 50.5 meV/atom more stable than the model *A*. The magnetic polarization in the model *A* can be expressed by the fraction of magnetic Mn atoms as $x_C = 5.4\%$. Model *B* is essentially nonmagnetic, $x_C = 0.006\%$. Hippert *et al.*[5] reported for *i*-Al-Pd-Mn samples of various composition a fraction of magnetic Mn atom x_C varying from 0.044% to 2.32%. A properly chosen mixed Al/Pd occupancy of the conflicting sites can thus provide agreement with experiment for any measured sample.

The sensitivity of the magnetic properties of measured samples to the content of Mn and Pd atoms observed by Hippert *et al.*[49] and reported also recently by Godonyuk *et al.*[51,57] indicates that the origin of the magnetism is indeed in Mn-Pd interaction as described above. The alternative mechanism for magnetic moment formation by a loosely packed environments of the Mn atoms plays obviously only a minor role.

V. DISCUSSION

We have presented a detailed *ab initio* spin-density-functional investigations of the magnetic properties of icosahedral Al-Pd-Mn quasicrystals. In contrast to earlier studies we find that in a model where all atoms occupy the ideal lattice sites derived within the Katz-Gratias-Boudard (KGB) model by projection from 6D hyperspace substantial magnetic moments exist on the majority of Mn atoms. The difference is due to a different initialization of the local magnetic moments (based on a series of fixed moment calculations) and the fact that within the local-spin-density approximation the paramagnetic state represents a metastable state, whereas it is instable in the semilocal generalized gradient approximation.

The strong magnetism of the idealized model contradicts the available experimental results; hence the challenge is rather why real Al-Pd-Mn quasicrystals are only weakly magnetic and why the average magnetization shows such a strong dependence on the exact chemical composition and the thermal history of the samples. A relaxation of the idealized model leading to a more compact atomic arrangement around the Mn-sites shows that the unrealistically loose packing in the idealized model favors moment formation. Large magnetic moments still exist on two types of Mn-sites [Mn(4) and Mn(34)] distinguished by the presence of two or more direct Pd-neighbors. If these Pd atoms are gradually replaced by Al (structural models *B* to *F*), the tendency to form magnetic moments on the Mn atoms is gradually reduced. If Mn atoms have no Pd nearest neighbors (model *B*) the *i*-Al-Pd-Mn quasicrystal is essentially nonmagnetic. Total energy calculations demonstrate that the model B with no direct Mn-Pd neighbors and a nonmagnetic ground state has the lowest energy of all tested configurations.

The chemical decoration has been discussed in relation to the shell structure of the atomic acceptance domains in 6D hyperspace and to the real-space structure of the quasicrystal as described in terms of inter-penetrating pseudo-Mackay clusters centered by Mn atoms and Bergman clusters centered by Pd. We show that chemical decoration determined by the shell structure of the triacontahedral acceptance domains of the KGB model lead to a local conflict with the cluster-based description: the triacontahedral acceptance domains (and the assumed chemical decoration of the Bergman clusters) place Pd atoms next to the Mn atoms in the centers of the pseudo-Mackay clusters where their regular chemical decoration would prefer an Al atom. In a real quasicrystal the occupation of these sites will vary with the exact chemical composition of the sample and its thermal history. Hence our analysis provides a convincing explanation of the experimentally observed variations in the magnetization of Al-Pd-Mn quasicrystals building principle. Real quasicrystals are predicted to be magnetically rather inhomogeneous, depending on the local occupancy of the nearest-neighbor sites on Mn by Pd or Al.

A difficult point requiring further analysis is the magnitude of the largest moments on the Mn sites and the distri-

bution of the Mn moments. In our calculations the value of the largest observed moments does not exceed $3\mu_B$. In addition to the large moments we have observed smaller, $|m| < 0.5\mu_B$, but non-negligible magnetic moments on some Mn atoms, for instance the moments of some Mn atoms in the models *A* or *E*. These smaller moments are probably caused by the interaction with other Mn atoms carrying large magnetic moments. The analysis of the experimental data was mostly based on the assumption that Mn atoms are either nonmagnetic or carry the largest spin-moment compatible with Hund's rule (i.e., $S=5/2$). From the experimentally detected nonlinearities in the temperature dependence of the susceptibility,[58] it was even suggested that in the icosahedral alloy, the magnetic moment of the Mn atoms varies between $6\mu_B$ and $7.5\mu_B$, i.e., it could be much higher than the magnetic moment of a free Mn atom of $5\mu_B$. Giant magnetic moments exceeding the limit set by Hund's rule raise different questions. It has been suggested that these large magnetic moments arise from ferromagnetically coupled pairs of nearest-neighbor Mn atoms[59] (evidently this requires that Mn nearest neighbors exist in the icosahedral phase; but this is in contradiction to all existing structural models[60]). As an alternative explanation[58] the formation of giant magnetic moments as in dilute alloys of Mn, Fe, or Co in highly polarizable hosts such as Pd or Rh has been invoked. In this case the magnetization induced on the surrounding host atoms is added to the moment of the magnetic atom. In these systems, the formation of a large induced magnetization cloud is well confirmed by DFT calculations.[61,62] In Al-Pd-Mn quasicrystals, however, our calculations show only a very weak induced magnetization on the Pd atoms.

So far we have not discussed the interaction between the magnetic moments on the Mn atoms. Except for model *B* with idealized coordinates, all Mn moments are ferromagnetically aligned. Experimental data suggest that Mn moments are weakly interacting.[5,63] The oscillatory character of the Ruderman-Kittel-Kasuya-Yoshida (RKKY) interaction of localized Mn moments mediated by the sea of nearly free conduction electrons can lead to antiferromagnetically coupled magnetic moments and consequently to a spin-glass ordering at low temperature.[5,49,64] Moments with antiferromagnetic polarization were confirmed also in our calculations (e.g., in Figs. 5 and 10). Hippert *et al.*[49] suggested that the random sign of the exchange interaction between the localized Mn moments with conduction electrons could explain the absence of magnetism in Al-Pd-Mn quasicrystal. In these cases the nonmagnetic ground state would result from the quenching of the magnetic moments due to the frustration of the exchange interactions, whereas our calculations show that the absence of magnetic moments is an inherent property of the chemical order in the ground-state configuration. A picture of the interaction of magnetic moments in *i*-Al-Pd-Mn mediated by the nearly free Al s,p electrons only does not seem to be complete. Pd atoms and their coordination to the Mn atoms play a dominant role in the formation of magnetic moments and may also mediate an interaction of distant magnetic moments.

ACKNOWLEDGMENTS

This work was supported by the Austrian Ministry for Education, Science and Art through the Center for Computational Materials Science. M.K. thanks support from the Grant Agency for Science of Slovakia (Grant No. 2/5096/25) and from the Slovak Research and Development Agency (Grant No. APVV-0413-06, CEX-Nanosmart). We thank M. Mihalkovič for numerous helpful discussions.

[1] J. J. Hauser, H. S. Chen, and J. V. Waszczak, Phys. Rev. B **33**, 3577 (1986).
[2] D. Shechtman, I. Blech, D. Gratias, and J. W. Cahn, Phys. Rev. Lett. **53**, 1951 (1984).
[3] W. W. Warren, H. S. Chen, and G. P. Espinosa, Phys. Rev. B **34**, 4902 (1986).
[4] A. Gozlan, C. Berger, G. Fourcaudot, R. Omari, J. C. Lasjaunias, and J. J. Préjean, Phys. Rev. B **44**, 575 (1991).
[5] F. Hippert, M. Audier, J. J. Préjean, A. Sulpice, E. Lhotel, V. Simonet, and Y. Calvayrac, Phys. Rev. B **68**, 134402 (2003).
[6] C. A. Swenson, T. A. Lograsso, N. E. Anderson, Jr., and A. R. Ross, Phys. Rev. B **70**, 094201 (2004).
[7] D. Rau, J. L. Gavilano, Sh. Mushkolaj, C. Beeli, M. A. Chernikov, and H. R. Ott, Phys. Rev. B **68**, 134204 (2003).
[8] M. A. Chernikov, C. Beeli, E. Felder, S. Buchi, and H. R. Ott, Phys. Rev. B **68**, 094202 (2003).
[9] F. Hippert, M. Audier, J. J. Préjean, A. Sulpice, V. Simonet, and Y. Calvayrac, J. Non-Cryst. Solids **334-335**, 403 (2004).
[10] J. Hafner and M. Krajčí, Phys. Rev. B **57**, 2849 (1998).
[11] F. Hippert, V. Simonet, G. Trambly de Laissardière, M. Audier, and Y. Calvayrac, J. Phys.: Condens. Matter **11**, 10419 (1999).
[12] V. Simonet, F. Hippert, M. Audier, and G. Trambly de Laissardière, Phys. Rev. B **58**, R8865 (1998).
[13] G. Trambly de Laissardière and D. Mayou, Phys. Rev. Lett. **85**, 3273 (2000).
[14] C. Brink-Shoemaker, D. A. Keszler, and D. P. Shoemaker, Acta Crystallogr. B **45**, 13 (1989).
[15] T. Hoshino, R. Zeller, P. H. Dederichs, and M. Weinert, Europhys. Lett. **24**, 495 (1993).
[16] M. Krajčí and J. Hafner, Phys. Rev. B **58**, 14110 (1998).
[17] K. Hiraga and W. Sun, Philos. Mag. Lett. **67**, 117 (1993).
[18] K. Hiraga, M. Kaneko, Y. Mtasuo, and S. Hashimoto, Philos. Mag. B **67**, 193 (1993).
[19] V. Simonet, F. Hippert, H. Klein, M. Audier, R. Bellissent, H. Fischer, A. P. Murani, and D. Boursier, Phys. Rev. B **58**, 6273 (1998).
[20] N. Jakse and A. Pasturel, Phys. Rev. B **76**, 024207 (2007).
[21] I. Turek, Ch. Becker, and J. Hafner, J. Phys.: Condens. Matter **4**, 7257 (1992).
[22] F. J. Himpsel, Phys. Rev. Lett. **67**, 2363 (1991).
[23] E. G. Moroni, G. Kresse, J. Hafner, and J. Furthmüller, Phys.Rev. B **56**, 15629 (1997).
[24] R. Hafner, D. Spišák, R. Lorenz, and J. Hafner, Phys. Rev. B **65**, 184432 (2002).

[25] G. Kresse and J. Hafner, Phys. Rev. B **49**, 14251 (1994).
[26] G. Kresse and J. Furthmüller, Comput. Mater. Sci. **6**, 15 (1996).
[27] G. Kresse and J. Furthmüller, Phys. Rev. B **54**, 11169 (1996).
[28] J. P. Perdew, J. A. Chevary, S. H. Vosko, K. A. Jackson, M. R. Pederson, D. J. Singh, and C. Fiolhais, Phys. Rev. B **46**, 6671 (1992).
[29] J. P. Perdew and Y. Wang, Phys. Rev. B **45**, 13244 (1992).
[30] P. E. Blöchl, Phys. Rev. B **50**, 17953 (1994).
[31] G. Kresse and D. Joubert, Phys. Rev. B **59**, 1758 (1999).
[32] S. H. Vosko, L. Wilk, and M. Nusair, Can. J. Phys. **58**, 1200 (1980).
[33] D. Hobbs, J. Hafner, and D. Spišák, Phys. Rev. B **68**, 014407 (2003).
[34] J. Hafner and D. Hobbs, Phys. Rev. B **68**, 014408 (2003).
[35] B. Canals and C. Lacroix, Phys. Rev. Lett. **80**, 2933 (1998).
[36] J. Hafner and D. Spišák, Phys. Rev. B **72**, 144420 (2005).
[37] J. X. Zheng-Johansson, O. Eriksson, B. Johansson, L. Fast, and R. Ahuja, Phys. Rev. B **57**, 10989 (1998).
[38] D. Spišák and J. Hafner, J. Phys.: Condens. Matter **11**, 6359 (1999).
[39] D. Spišák and J. Hafner, Phys. Rev. B **61**, 11569 (2000).
[40] Ch. Becker, J. Hafner, and R. Lorenz, J. Magn. Magn. Mater. **157-158**, 619 (1996).
[41] P. H. Dederichs, S. Blügel, R. Zeller, and H. Akai, Phys. Rev. Lett. **53**, 2512 (1984).
[42] A. R. Williams, V. L. Moruzzi, J. Kübler, and K. Schwarz, Bull. Am. Phys. Soc. **29**, 278 (1984).
[43] K. Schwarz and P. Mohn, J. Phys. F: Met. Phys. **14**, L129 (1984).
[44] M. Cornier-Quiquandon, A. Quivy, S. Lefebvre, E. Elkaim, G. Heger, A. Katz, and D. Gratias, Phys. Rev. B **44**, 2071 (1991).
[45] A. Katz and D. Gratias, J. Non-Cryst. Solids **153-154**, 187 (1993).
[46] M. Boudard, M. de Boissieu, C. Janot, G. Heger, C. Beeli, H.-U. Nissen, H. Vincent, R. Ibberson, M. Audier, and J. M. Dubois, J. Phys.: Condens. Matter **4**, 10149 (1992).
[47] M. de Boissieu, P. Stephens, M. Boudard, C. Janot, D. L. Chapman, and M. Audier, J. Phys.: Condens. Matter **6**, 10725 (1994).
[48] M. Krajčí, M. Windisch, J. Hafner, G. Kresse, and M. Mihalkovič, Phys. Rev. B **51**, 17355 (1995).
[49] F. Hippert and J. J. Préjean, Philos. Mag. (to be published).
[50] A. Sadoc and J. M. Dubois, J. Non-Cryst. Solids **153-154**, 83 (1993).
[51] A. Godonyuk, E. Isaev, and Y. Kh. Vekilov, Philos. Mag. **88**, 2191 (2008).
[52] M. Mihalkovič and M. Widom, alloy database at http://alloy.phys.cmu.edu/.
[53] V. Elser, Philos. Mag. B **73**, 641 (1996).
[54] D. Gratias, F. Puyraimond, M. Quiquandon, and A. Katz, Phys. Rev. B **63**, 024202 (2000).
[55] M. Krajčí, J. Hafner, J. Ledieu, and R. McGrath, Phys. Rev. B **73**, 024202 (2006).
[56] A. Quandt and V. Elser, Phys. Rev. B **61**, 9336 (2000).
[57] A. Godonyuk, E. Isaev, and Y. Vekilov, J. Magn. Magn. Mater. **300**, e567 (2006).
[58] K. Fukamichi, in *Physical Properties of Quasicrystals*, edited by Z. M. Stadnik, Solid State Sciences Vol. 128 (Springer, Berlin, 1999), p. 295.
[59] C. Berger and J. J. Préjean, Phys. Rev. Lett. **64**, 1769 (1990).
[60] M. Quiquandon and D. Gratias, Phys. Rev. B **74**, 214205 (2006).
[61] S. Dennler, J. Hafner, M. Marsman, and J. Morillo, Phys. Rev. B **71**, 094433 (2005).
[62] J. Hafner and D. Spišák, Phys. Rev. B **76**, 094420 (2007).
[63] J. J. Préjean, E. Lhotel, A. Sulpice, and F. Hippert, Phys. Rev. B **73**, 214205 (2006).
[64] D. Rau, J. L. Gavilano, Sh. Mushkolaj, C. Beeli, and H. R. Ott, J. Magn. Magn. Mater. **272-276**, 1330 (2004).